Electronic Supplementary Information (ESI)

Visible-light driven CO_2 photoreduction over $Zn_xCd_{1-x}S$ solid solution coupling with tetra(4-carboxyphenyl)porphyrin iron(III) chloride

Pan Li,[a,c] Xuehua Zhang,*[a] Chunchao Hou,[b] Lin Lin,[a] Yong Chen*[b,c] and Tao He*[a,c]

[a] CAS Key Laboratory of Nanosystem and Hierarchical Fabrication, CAS Center for Excellence in Nanoscience, National Center for Nanoscience and Technology, Beijing 100190, China.

[b] Key Laboratory of Photochemical Conversion and Optoelectronic Materials, Technical Institute of Physics and Chemistry, Chinese Academy of Sciences, Beijing 100190, China.

[c] University of Chinese Academy of Sciences, Beijing 100049, China

Chemicals

All of the chemicals and solvents used were analytical grade or chromatographic grade. $Zn(NO_3)_2\cdot 6H_2O$ and $Cd(NO_3)_2\cdot 4H_2O$ were purchased from Shanghai Macklin biochemical technology Co., LTD. $CS(NH_2)_2$ was bought from Jingke Fine Chemical Industry Research Institute of Tianjin. Triethanolamine (TEOA, 99.8%, GC), acetonitrile (MeCN, 99.9%, GC) and ethylenediamine (> 99%) were purchased from Shanghai Aladdin Bio-chem Technology. Carbon dioxide gas (super grade purity 99.999%) was bought from Beijing Beiwen Gases Company. The high-purity water used was purified by a Milli-Q Plus system (Millipore, France) with 18.2 MΩ·cm resistivity in all the experiments.

Characterizations

The morphology and element mapping analysis were obtained by using Hitachi S4800 field emission scanning electron microscope (FESEM) and Tecnai G2 F20 U-TWIN transmission electron microscopy (TEM). Powder X-ray diffraction (XRD) was carried out on a Bruker D8 diffractmeter with Cu Kα radiation. UV-vis diffuse reflectance spectroscopy (DRS) and UV-vis absorption spectra were collected on Lambda 750 UV/Vis/NIR spectrophotometer (Perkin-Elmer, USA) using $BaSO_4$ as the background. The valence band position of the products was obtained from X-ray photoelectron spectroscopy (XPS) using ESCALAB 250Xi X-ray photoelectron spectrometer. Fourier transform infrared (FT-IR) absorption spectra were performed on a Perkin Elmer spectrometer. The BET specific surface area and carbon dioxide adsorption isotherms were obtained by a surface area and porosity analyzer

(Micromeritics, Tristar II 3020). Photoluminescence (PL) spectra were collected excited at 350 nm, and the time-resolved PL spectra were recorded with 375 nm excitation at room temperature on spectrometer (FLS920, Edinburgh Instruments). Electron spin resonance (ESR) signals were recorded with a Bruker E500 spectrometer at room temperature. Inductively coupled plasma-mass spectrometry (ICP-MS) was carried out on NexION 300X (Perkin-Elmer, USA). The respective concentration of Zn and Cd for ZCS-1 is thus determined to be 3.93 and 43.29 μg/L, and it is 6.56 and 41.31 μg/L for ZCS-2. The Mott-Schottky (M-S) curves were collected in a three-electrode cell on CHI 660D electrochemical station (Shanghai Chenhua, China) with a frequency of 1 kHz. The as-prepared samples, Pt foil and saturated calomel electrode (SCE) were used as the working, counter and reference electrodes, respectively.

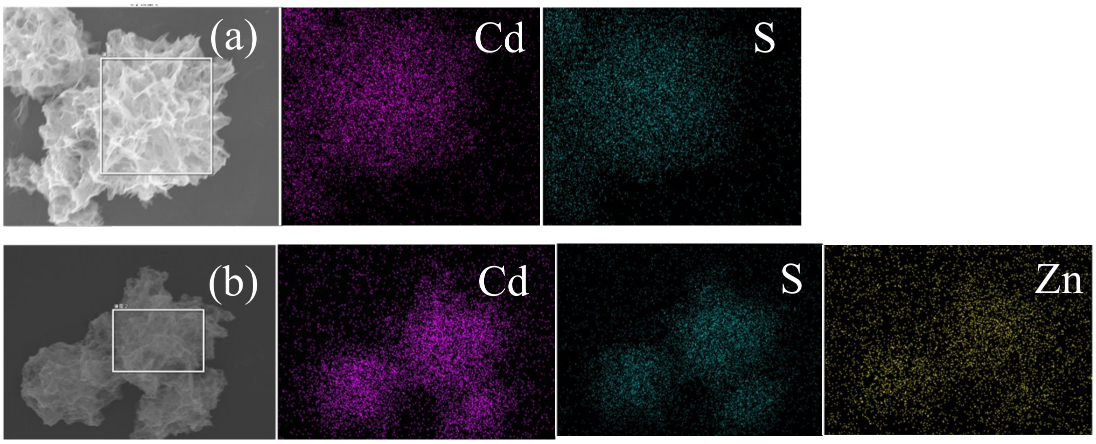

Figure S1. EDX mapping of (a) CdS and (b) ZCS-2, obtained from SEM analysis.

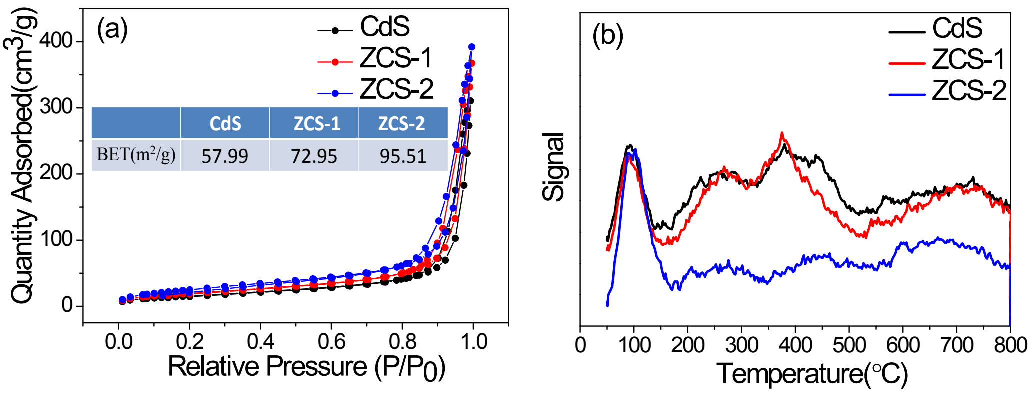

Figure S2. (a) Typical N_2 adsorption-desorption isotherm and (b) CO_2 chemical adsorption isotherm of CdS, ZCS-1 and ZCS-2.

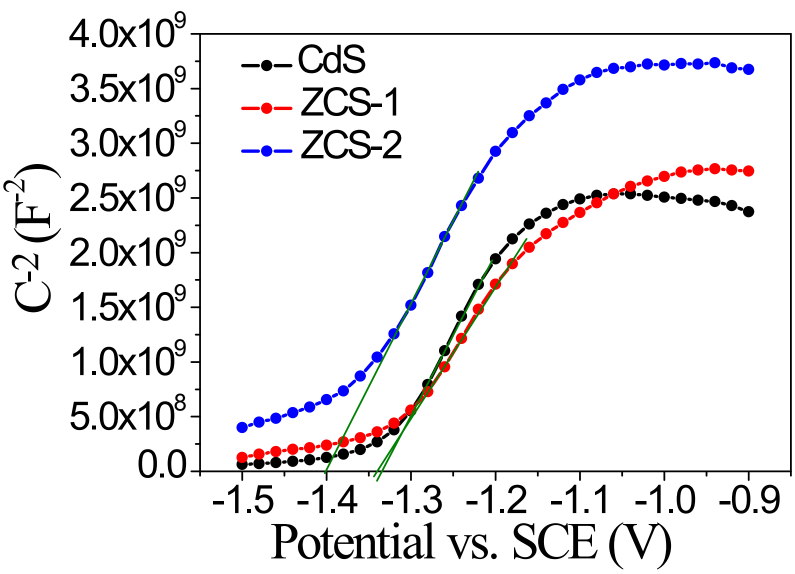

Figure S3. Mott-schotty (M-S) plots of CdS, ZCS-1 and ZCS-2, which were measured to determine the flatband potential (E_{FB}) of CdS, ZCS-1 and ZCS-2, using the equation of $\frac{1}{C^2} = \frac{2}{\varepsilon\varepsilon_0 N_D}\left(E - E_{FB} - \frac{k_B T}{q}\right)$, where C is space charge capacitance, N_{D} is the donor density, ε and ε_0 are the respective dielectric constants of free space and the film electrode, E is the applied potential, E_{FB} is the flat-band potential, κ_{B} is Boltzmann's constant, T is the temperature, and q is the electronic charge. The E_{FB}

values can be estimated from the intercept at X axis of M-S curves by linear extrapolation of the linear region ($1/C^2 = 0$), which are −1.33 V, −1.34 V, and −1.40 V (vs. SCE), corresponding to −1.09 V, −1.10 V, and −1.16 V (vs. NHE) for CdS, ZCS-1 and ZCS-2, respectively. All the E_{FB} values are negative than the reduction potential of FeTCPP ($E_{Fe}^{I/0}$, −1.02 V vs NHE), implying that the electron transfer from both CdS and ZCS to FeTCPP is thermodynamicly feasible. Moreover, the E_{CB} of a n-type semiconductor is higher than its E_{FB}, usually 0.1~0.3 eV more, dependent on the electron effective mass and carrier concentration. [S1,S2] If the difference between E_{CB} and E_{FB} is set to be 0.2 eV, the E_{CB} bottom for CdS, ZCS-1 and ZCS-2 is −1.29 V, −1.30 V, and −1.36 V, respectively. Thus, M-S results further prove that the electron can transfer from both CdS and ZCS to FeTCPP.

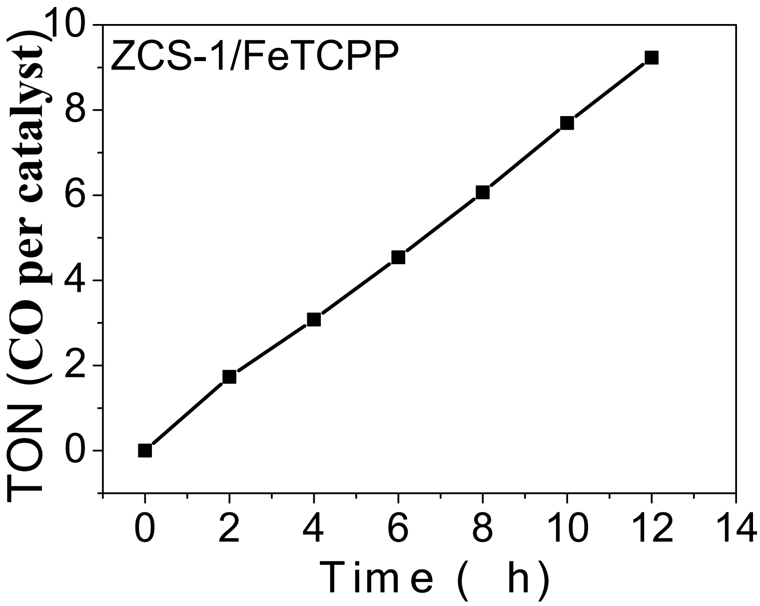

Figure S4. TON vs time plot of ZCS-1/FeTCPP hybrid system.

The TON value vs time plots of ZCS-1/FeTCPP hybrid system was calculated based on the FeTCPP amount. The TON is around 9.2 after 12 h. It is noted that this number is not very high. However, this system does show the advantage of good stability and low cost. It should be pointed out that this work mainly focuses on “the introduction of appropriate amount of Zn into CdS can change the charge separation efficiency, strengthen the coupling of CdS with FeTCPP, and build effective interfacial channels for electron transfer from ZCS to FeTCPP”. Based on this, we believe that the photocatalytic activity of CO_2 reduction would be greatly increased in future via molecularly tailoring of the FeTCPP catalysts and/or the interfacial modulation.

Stability of the ZCS solid solution

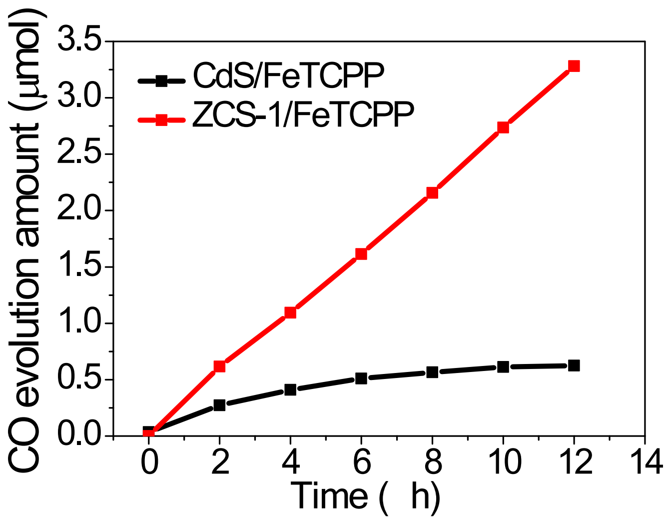

Figure S5. Time dependence of CO evolution amount upon CO_2 photoreduction using CdS/FeTCPP and ZCS-1/FeTCPP catalysts in CH_3CN: H_2O: TEOA (3:1:1, 100 mL) mixed solution under visible-light illumination for 12 h.

In addition to the photocatalytic activity, the stability is another important issue for evaluation of the photocatalysts. The CO yield increases linearly within 12 h for the ZCS-1/FeTCPP hybrid system, while the CO production over CdS/FeTCPP increases nonlinearly as the time extends and eventually tends to a “constant” value, indicating higher stability of ZCS-1/FeTCPP than that of CdS/FeTCPP. XPS characterization of the ZCS samples before and after CO_2 photoreduction has been performed. As shown in Fig. S6, the binding energy of Cd3d and S2p for ZCS-1 and ZCS-2 samples keeps unchanged after reduction experiment; while the binding energy for both Cd3d and S2p in CdS is changed. Moreover, considering the ZCS-1/FeTCPP hybrid system is still efficient after 12 h illumination (Fig. S5), the deactivation of the CdS/FeTCPP hybrid system may originate from the instability of CdS, rather than the deactivation of FeTCPP.

In this work, the stability of ZCS solid solution was also evaluated by XRD, XPS and SEM investigation after CO_2 photoreduction. The XRD patterns of ZCS after photoreduction are similar to those before the experiments (Figure S6). The original wurtzite structure is also kept quite well upon CO_2 reduction. Furthermore, the XPS analysis was also used to probe surface chemical states of the photocatalysts. Figure S6(b-d) exhibits high-resolution spectra of Zn 2p, Cd 3d, and S 2p in ZCS solid solution samples before and after photoreduction. It is found that some changes happened to pure CdS after CO_2 photoreduction, indicating the pure CdS is not so stable even though in the presence of TEOA as sacrifice agent. However, such phenomenon cannot be observed from XRD analysis due to the detection limit of XRD. Interestingly, after introducing Zn into CdS forming the ZCS solid solution, all of the XPS and XRD peaks exhibit almost no change upon CO_2 photoreduction, which implies the stability of CdS upon the photocatalytic reaction can be enhanced via the formation of ZCS solid solution. In addition, as shown in Figure S7, the morphology of all the ZCS samples is kept quite well during the process of photocatalytic reduction.

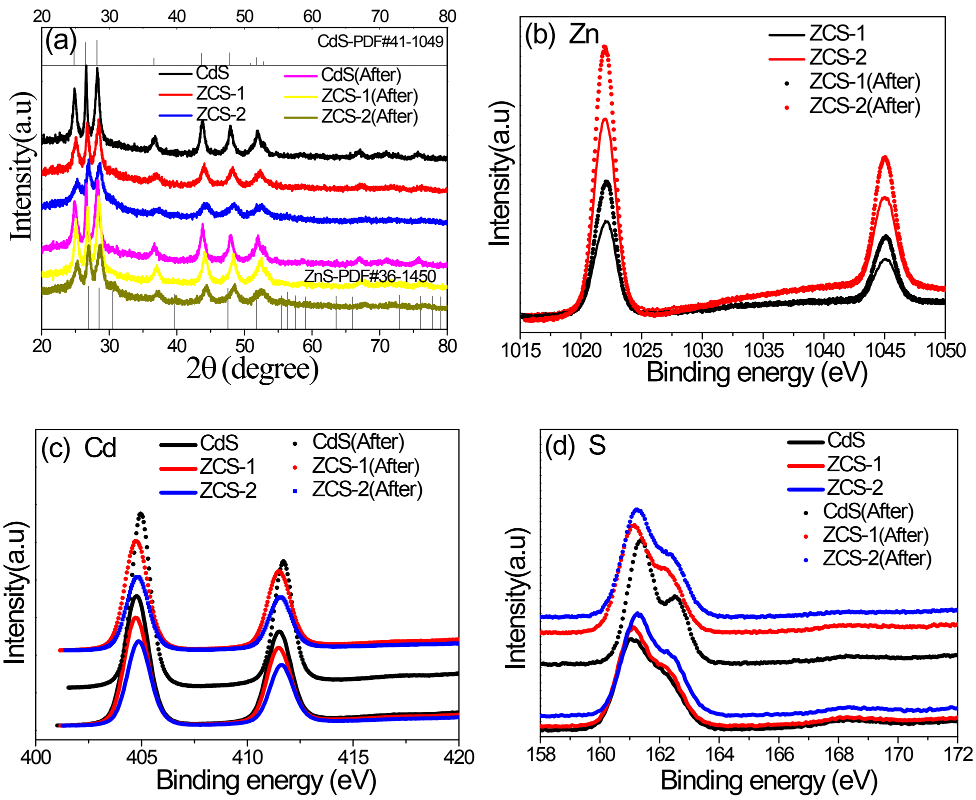

Figure S6. (a) XRD patterns and (b)-(d) XPS spectra of the synthesized ZCS samples after CO_2 photoreduction.

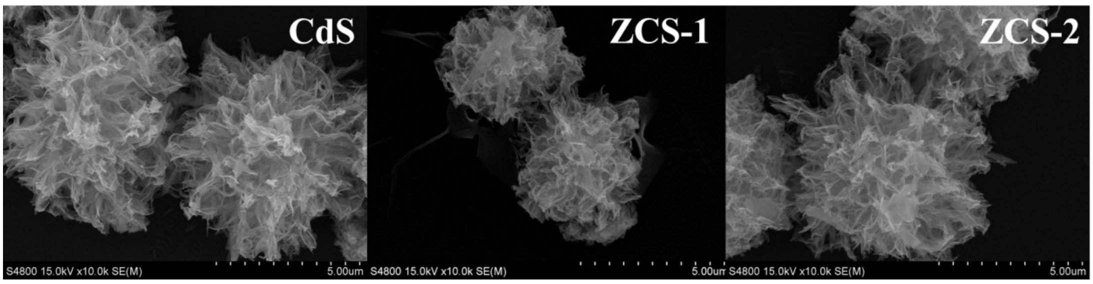

Figure S7. SEM images of the synthesized ZCS samples after CO_2 photoreduction.

Table S1. The element composition, BET surface area, and CO_2 chemical adsorption amount of CdS, ZCS-1 and ZCS-2.

Sample	CdS	ZCS-1	ZCS-2
Element composition from SEM	$Cd_{0.97}S$	$Zn_{0.14}Cd_{0.84}S$	$Zn_{0.23}Cd_{0.83}S$
Element composition from TEM	$Cd_{0.92}S$	$Zn_{0.14}Cd_{0.82}S$	$Zn_{0.21}Cd_{0.75}S$
BET surface area (m^2/g)	57.99	72.95	95.51
CO_2 chemical adsorption (cm^3/g)	10.52	18.06	14.13

Table S2. Atomic ratio of Zn and Cd in the ZCS-1 and ZCS-2 samples, obtained from SEM-EDX, TEM-EDX and ICP-MS results, respectively.

	ZCS-1	ZCS-2
Zn/Cd from SEM-EDX	0.167	0.277
Zn/Cd from TEM-EDX	0.171	0.280
Zn/Cd from ICP-MS	0.160	0.272

References:

S1. N. Tian, H. W. Huang, C. Y. Liu,; F. Dong, T. R. Zhang, X. Du, S. X. Yu and Y. H. Zhang, *J. Mater. Chem. A*, 2015, **3**, 17120–17129.

S2. W. J. Luo, Z. S. Li, X. J. Jiang, T. Yu, L. F. Liu, X. Y. Chen, J. H. Ye and Z. G. Zou, *Phys. Chem. Chem. Phys.*, 2008, **10**, 6717–6723.